Estuaries and Coasts
https://doi.org/10.1007/s12237-020-00778-1

Contrasting Radium-Derived Groundwater Exchange and Nutrient Lateral Fluxes in a Natural Mangrove Versus an Artificial Canal

Praktan D. Wadnerkar[1] · Bayartungalag Batsaikhan[2] · Stephen R. Conrad[1] · Kay Davis[1] · Rogger E. Correa[1,3] · Ceylena Holloway[1] · Shane A. White[1] · Christian J. Sanders[1] · Isaac R. Santos[1,4]

Received: 27 January 2020 / Revised: 4 May 2020 / Accepted: 8 June 2020

Abstract

Artificial canals may function differently than the natural coastal wetlands, floodplains, and estuaries they often replace. Here, we assess the impact of canal estate development on saline groundwater exchange (tidal pumping) and associated nutrient fluxes. Time series observations of short-lived radium isotopes and dissolved nutrients were performed in a canal estate and a nearby mangrove creek in subtropical Australia. A mass balance model based on ^{223}Ra (1.3 ± 0.4 and 3.4 ± 0.9 cm day^{-1} in the mangrove and canal, respectively) and ^{224}Ra (2.8 ± 3.0 and 5.4 ± 4.6 cm day^{-1}) revealed tidally driven groundwater exchange rates were ~ 2-fold greater in the canal. Lateral fluxes of total dissolved nitrogen (TDN) from the nearby estuary into the canal estate were comparable with the mangrove creek (8.4 and 9.1 mmol m^{-2} day^{-1} in the mangrove and canal, respectively). Groundwater flows into the canal released ~ 5-fold more TDN than the mangrove. As expected, mangroves appear to be more efficient at retaining groundwater-derived nitrogen than vegetation-stripped, sandy canals. Overall, this study demonstrates that land reclamation for canal estate development not only drives losses of ecosystem services, but also modifies groundwater and related nutrient exchange with coastal surface waters.

Keywords Eutrophication · Blue carbon · Coastal carbon · Submarine groundwater discharge · Porewater

Introduction

Coastal canal estates are often built by dredging and reclaiming natural intertidal saltmarsh-mangrove areas, or constructed in nearby floodplains beyond the high tide mark (Davis et al. 2020; Macklin et al. 2017; Trent et al. 1972). Artificially constructed canal estate waters can function differently than the wetland and floodplain habitats they replace (Balfour et al. 2012; Cook et al. 2007; Morton 1992). Canals are often dredged to make deeper waters, disturbing soil strata, increasing untreated land runoff, and influencing surface water circulation (Morton 1989; Stocker et al. 2016). Complex engineered designs and altered connectivity to main waterways can decrease flushing in canals (Benfer et al. 2010; Macklin et al. 2017). In tropical and subtropical regions, coastal canals often displace intertidal mangrove wetlands.

Mangrove wetlands are one of the most productive biomes on the planet (Alongi et al. 2002; Reef et al. 2010; Wang et al. 2010). Mangrove ecosystems can create a suitable environment to remove or attenuate water pollutants (Adame et al. 2019; Leung et al. 2016), sequester nutrients and carbon (Sanders et al. 2016; Wadnerkar et al. 2019), protect shorelines from erosion (Gedan et al. 2011), maintain high levels of biodiversity (Macintosh and Ashton 2002), and provide resources to coastal communities (Macnae 1969; Zedler and Kercher 2005). The dominant benthic fauna is associated with mangrove forests (i.e., crabs), bury, ingest litter, and microalgal mats (Kristensen 2008; Kristensen and Alongi 2006; Reef et al. 2010), preventing loss of nutrients and promoting recycling. Crab burrows also affect sediment topography and biogeochemistry by modifying drainage, particle size distribution, nutrient dynamics, and groundwater exchange (Kristensen 2008; Ridd 1996; Xin et al. 2009).

Communicated by Nancy L. Jackson

✉ Praktan D. Wadnerkar
praktan.wadnerkar@scu.edu.au

[1] National Marine Science Centre, Southern Cross University, Coffs Harbour, New South Wales, Australia

[2] Institute of Geography and Geoecology, Mongolian Academy of Sciences, Ulan Bator, Mongolia

[3] Corporación Merceditas - Merceditas Corporation, Medellín 050021, Colombia

[4] Department of Marine Sciences, University of Gothenburg, Gothenburg, Sweden

Published online: 28 July 2020

Submarine groundwater discharge (SGD) or groundwater exchange can be important pathways for solute delivery to the coastal ocean in the subtropical and tropical estuarine waters surrounded by mangrove ecosystems (Chen et al. 2018; Taillardat et al. 2018). Tidally driven SGD flushes crab burrows in mangrove sediments, supplying dissolved organic and inorganic nutrients to coastal waters (Santos et al. 2019; Stieglitz et al. 2013; Tait et al. 2017). In some cases, saline SGD can facilitate the removal or consumption of carbon and nitrogen in coastal sediments (Robinson et al. 2018). Therefore, destruction or modification of mangroves in subtropical estuaries can have a substantial effect on coastal biogeochemical cycles and SGD (Alongi 2002; Wang et al. 2010; Zedler and Kercher 2005). Groundwater flows can be enhanced in areas with disturbed drainage such as canals and drains (Burnett et al. 2010; Cardwell et al. 1980; De Weys et al. 2011; Macklin et al. 2014).

Natural geochemical tracers, such as radium radioisotopes (^{223}Ra, ^{224}Ra, ^{226}Ra, and ^{228}Ra), are widely used to quantify SGD at the ecosystem scale (Burnett et al. 2006; Moore and Arnold 1996; Sadat-Noori et al. 2017). Radium isotopes are enriched in brackish/saline groundwater and conservative in seawater once released from groundwater (Burnett et al. 2006). However, radium isotopes may not be enriched in freshwater discharge such as submarine springs (Burnett et al. 2006). The two radium isotopes with the shortest half-lives (^{224}Ra half-life = 3.66 days, ^{223}Ra half-life = 11.4 days) are suitable to investigate short scale processes such as tidally driven SGD and coastal mixing (Garcia-Orellana et al. 2010).

Here, we hypothesize that the replacement of mangroves by artificial canals alters SGD and the exchange of nutrients between intertidal zones and the coastal ocean. We use ^{223}Ra and ^{224}Ra to estimate saline SGD and related nutrient loading in an artificial canal and a nearby mangrove creek. We build on earlier investigations revealing how artificial canals and drains may be hotspots of groundwater-surface water connectivity in coastal canals in Australia (Davis et al. 2020; Macklin et al. 2014), the Everglades wetland in Florida (Choi and Harvey 2000; Harvey et al. 2005), and coastal acid sulfate soil (CASS) drainage networks (Santos et al. 2013; Webb et al. 2017). Our concurrent observations at the two nearby systems ensure that natural temporal variability is not an influencing factor, allowing a direct comparison between the mangrove and canal systems.

Material and Methods

Study Site

Field investigations were concurrently performed in a waterfront canal estate (Yamba Quays) and a nearby mangrove creek along the Oyster Channel of the Clarence River in Yamba, New South Wales, Australia (Fig. 1a, b). Yamba has a population of ~ 6100 (Bureau of Statistics 2017). The two water systems are located only ~ 1 km apart and drain to the Clarence River estuary approximately 3 km upstream of its confluence with the Pacific Ocean. Both sites receive urban runoff during rain events, though this was not observed during our field work due to dry conditions. The area has a humid subtropical climate and receives an average yearly precipitation of ~ 1100 mm (BOM 2017) with a mild monsoon season from February to April. Air temperature ranges from 10 to 30 °C. The canal is surrounded by waterfront houses built on elevated land that was formerly an intertidal system. Dredging and development of the canal estate started in 1997 and finished by the end of 2001. Canal banks are either covered by fine silty sands or reinforced with concrete retaining walls while the mangrove creek sediments are silt and clay with intermittent sand patches. The canal has steeper banks (21%) compared with mangrove (8%). Tidal waters infiltrate crab burrows in the mangrove site, whereas crab burrows were absent in the sandy canal beaches.

Surface Water Time Series

Two time series stations (Fig. 1) were set up at the mouth of the canal and mangrove creek to compare (1) radium-derived groundwater exchange, (2) the related input of nutrients to surface waters, and (3) lateral nutrient exports to the coastal ocean. Time series observations were conducted at both sites simultaneously for 36 h from 04:00 June 14 to 16:00 June 15, 2018. Our strategy removes temporal biases, allowing for direct comparisons to be made between the two sites.

Radium and nutrient samples were collected every 1 h for 36 h, covering 3 complete tidal cycles. Water for radium capture was collected in 100-L containers and drained through manganese (Mn) fibers that absorb dissolved radium from seawater (Moore 2010). In the laboratory, fibers were washed with radium-free water to remove salt particles and analyzed with a Radium Delayed Coincidence Counter (RaDeCC) for ^{223}Ra and ^{224}Ra activities (Moore 2010). After > 21 days (> 6 half-lives of ^{224}Ra), the fibers were re-analyzed with the RaDeCC for ^{228}Th. Results reported here represent excess ^{224}Ra after correction for ^{228}Th decay (Garcia-Solsona et al. 2008).

For nutrient analysis, samples were immediately filtered using 0.45-μm cellulose acetate syringe filters into sample-rinsed 10-mL polyethylene vials, kept on ice for less than 3 h, then stored at − 5 °C until analysis (White et al. 2018). Analyses for ammonium (NH_4), nitrate plus nitrite (NO_x), phosphate (PO_4), and total dissolved nitrogen (TDN) were carried out colorimetrically using a flow injection analyzer (FIA) with precision better than 5%. Subtracting NO_x and NH_4 from TDN determined dissolved organic nitrogen (DON) concentrations. At both sites, a calibrated Hydrolab MS5 sonde logged temperature (°C), dissolved oxygen (DO,

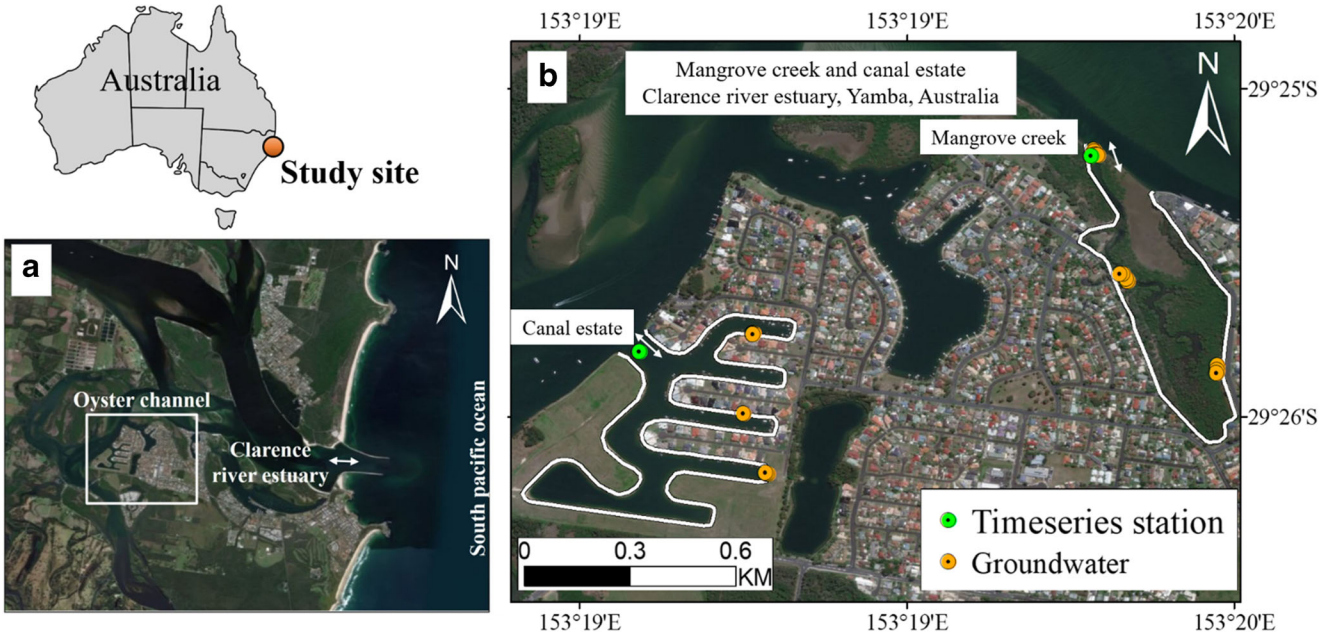

Fig. 1 **a** Oyster Channel, Clarence River estuary, Yamba. **b** Canal estate and mangrove dominated creek, Clarence River estuary, Yamba, Australia. Green circles show the locations of the surface water time series station. Groundwater samples were taken from the canal and mangrove (orange circles)

in mg L^{-1}), pH and salinity every 60 min, and a CTD (vanEssen instruments) measured water depth every 10 min.

A groundwater spatial survey was undertaken following the surface water time series experiments to characterize the seeping radium and nutrient endmembers in close proximity to the canal ($n = 6$) and mangrove creek ($n = 11$). One to two-meter shallow boreholes were dug with a hand auger within the intertidal zone along the mangrove creek and canal estate (Fig. 1). A slotted 50-mm polyvinyl chloride (PVC) pipe was inserted in the borehole to contain the pump hose and allowed to fill with groundwater. The pipe was pumped and allowed to refill several times prior to sampling using a peristaltic pump (Atkins et al. 2013). Samples were collected and analyzed for nutrients and radium isotopes as above.

Diffusion Experiment

A total of four surface sediment samples, two coarse grained (sandy) from canal site and two fine grained (muddy) from mangrove creek sites, were collected to estimate diffusive fluxes of ^{223}Ra and ^{224}Ra and build mass balances. Sediments were spread uniformly over the bottom of a 20-L plastic container. A total of 10 L of Ra-free water (salinity ~ 32 comparable with the field salinity) was delivered into the containers, minimizing sediment disturbance. An air bubbler was placed in the container to provide oxygen to the water and avoid changes in redox characteristics. The container was sealed with a plastic lid to minimize water loss via evaporation. The sediment was left to incubate for at least 82 days (> 6 half-lives of ^{223}Ra). The water covering the sediment was then removed and filtered through manganese fibers for later analysis. The diffusive fluxes were assumed to be equivalent to the decay flux of short-lived radium isotopes after secular equilibrium was reached in the overlying water (Stewart et al. 2015).

Radium Isotope Mass Balance

A ^{223}Ra and ^{224}Ra mass balance model was developed considering all sources and sinks of radium isotopes and estimate SGD. Surface water fluxes were integrated over a 36-h tidal cycle following a mass balance approach:

$$\int_0^{36}(F_{\mathrm{ft}}\mathrm{Ra}_{\mathrm{ft}} - F_{\mathrm{et}}\mathrm{Ra}_{\mathrm{et}}) + F_{\mathrm{gw}}\mathrm{Ra}_{\mathrm{gw}} + \mathrm{Ra}_{\mathrm{diff}}A\lambda - \mathrm{Ra}V\lambda = 0 \quad (1)$$

where Ra_{gw} is the average groundwater concentration (dpm m^{-3}) minus the high tide surface water concentration; this approach assumes tidally driven seawater circulation in beach sediments is the main source of radium to surface waters as discussed below; $\mathrm{Ra}_{\mathrm{diff}}$ is the diffusion from bottom sediments (dpm m^{-3}); A is the surface area of the system during high tide measured using the GIS ArcMap 10 software (m^2); λ is the radium decay constant (0.06 unit day^{-1}); $F_{\mathrm{ft}}\mathrm{Ra}_{\mathrm{ft}}$ is the radium input flux during flood tide (dpm h^{-1}); and $F_{\mathrm{et}}\mathrm{Ra}_{\mathrm{et}}$ is the radium flux during ebb tide (dpm h^{-1}). $\mathrm{Ra}V\lambda$ is the radium decay, where Ra is the concentration, V is the surface water volume (m^3) calculated with surface area and depth (determined using a Garmin depth sounder), and λ is the radium decay constant (0.0608 day^{-1} for ^{223}Ra and 0.1893 day^{-1} for ^{224}Ra). The ^{223}Ra/^{224}Ra

activity ratio at both sites was similar (0.04 ± 0.01 and 0.05 ± 0.02), which indicates the main source of the radium is the same. The radium decay constant is a function of the isotope half-life, i.e., $\lambda = \frac{\ln(2)}{T_{1/2}}$ where $T_{1/2}$ ^{224}Ra is 3.6 days and 11.4 days for ^{223}Ra. Since there were no fresh surface water inputs during the time series, we neglect desorption of suspended sediment particles as a radium source. All the terms in the mass balance were estimated and the equation was solved for groundwater exchange (F_{gw})after integration over 36 h (3 tidal cycles).

Our model assumed that tidal input, groundwater, and diffusion from sediments were the only sources of radium isotopes during the 36-h integration period (Gleeson et al. 2013). By integrating three complete tidal cycles, the model accounts for all fluxes occurring over the 36-h integration period, but cannot quantify fluxes over time scales shorter than one tidal cycle. Our model is different than non-steady state radon mass balance models often applied to continuous time series datasets that estimate SGD at hourly time scales in open shorelines (Burnett and Dulaiova 2003; Santos et al. 2009). Our integration approach is ideal for enclosed tidal basins with a single opening. By calculating the net SGD tracer flux out of the confined tidal basins based on detailed observations, we avoided the need for estimating the return flow factor or flushing times. These terms often introduce large uncertainties to tracer mass balance models (Moore et al. 2006) and are not available for our study sites. The tidal prism is the volume of water penetrating the canal or mangrove at each tidal cycle. Here, we used changes in water level and volume over time to estimate fluxes in and out of the systems (F_{ft} and F_{et}) at 1 hour time steps.

A detailed spatial survey was conducted to measure the depth and volume of the canal using a Garmin depth sounder with observations spaced 3–10 m apart and depth precision of 10 cm for individual readings. We also deployed depth loggers at the mouth and upper end of both mangrove and canal system (data not shown). Because of the small size of both systems (< 2 km in length), the change in tides at the mouth and upper limit of both systems was homogenous, building confidence in our tidal prism-based model of surface water flows. Our approach assumes that the depth in the small restricted systems was spatially homogenous. Positive changes in water depth (flood tide) yield negative flows, whereas negative changes in water depth (ebb tide) yield positive flows out of the system.

Lateral Exports and Groundwater Nutrients

Lateral nutrient exports to the coastal ocean were estimated by multiplying water flow by the nutrient concentrations at the surface water stations and integrating the hourly time steps over 36 h of observations (Gleeson et al. 2013). To estimate SGD-derived nutrient fluxes, we multiplied the radium-derived SGD rate by the groundwater nutrient endmember. Because tidally driven seawater recirculation in sediments controls SGD in the two systems (discussed below), nutrient concentrations in groundwater were subtracted from average high tide surface water concentrations to define the groundwater endmember (Smith and Swarzenski 2012). This approach prevents us from overestimating endmember concentrations by including only the net change in nutrient concentration within sediments under the assumption that saline SGD dominates fresh SGD (Santos et al. 2019).

Uncertainties in calculated data (e.g., SGD estimates, surface water nutrient loads, and SGD-derived nutrient fluxes) were determined by propagating the errors associated with each individual term (Harvard 2007) following recommendations from Sadat-Noori et al. (2015).

Results

Time Series Observations

Mean water volume in the canal was ~ 12-fold higher than the mangrove creek due to dredging of the canal for recreational vessel navigation. Conversely, the mangrove intertidal area was ~ 8-fold greater than the canal (Table 1). Therefore, dilution of surface water is more prominent in the canal due to small intertidal area relative to its volume. As a result, radium concentrations in the mangrove surface water and groundwater are higher than the canal while fluxes are higher in the canal than in the mangrove. The area received 13.4 mm of rainfall in 5 days prior to the time series experiments. No rainfall occurred during the time series experiment (BOM 2019) and no surface runoff was observed during the experiments, simplifying the interpretation of our observations.

Salinity in the mangrove creek and canal varied between 28 and 34 with an average of ~32 (Fig. 2). A significant difference between the two sites was surface water nutrient concentrations and temporal trends. NH_4 was the dominant

Table 1 Basic characteristics of mangrove and canal sites

	Unit	Mangrove	Canal
Surface area at high tide	km^2	0.05	0.14
Intertidal area	km^2	0.1	0.02
Perimeter length at low tide	km	2.2	4.1
Average volume	m^3	24,420	237,030
Average depth	m	0.7	2.0
Tidal range	m	1.2	1.2
Salinity		31.8	32.8
Temperature	°C	18.9	19.0
Sediment composition		Clay, silt, and sand	Sand

form of nitrogen at both time series stations (~ 70 ± 18% of TDN) (Fig. 3 and Table 2) with DON also present in a large proportion (23 ± 20% of TDN) (Fig. 3). The DIN:DIP ratio was close to the Redfield ratio in both the mangrove creek (17.6:1) and the canal (14.0:1). Nutrients and radium isotopes had clear tidal trends in the mangrove creek, but not in the canal (Fig. 2). Radium concentrations followed an inverse tidal trend at both sites and were clearly seen to have the highest values at the lowest tide. These tidal trends in activities imply enhanced groundwater discharge at low tide and mixing

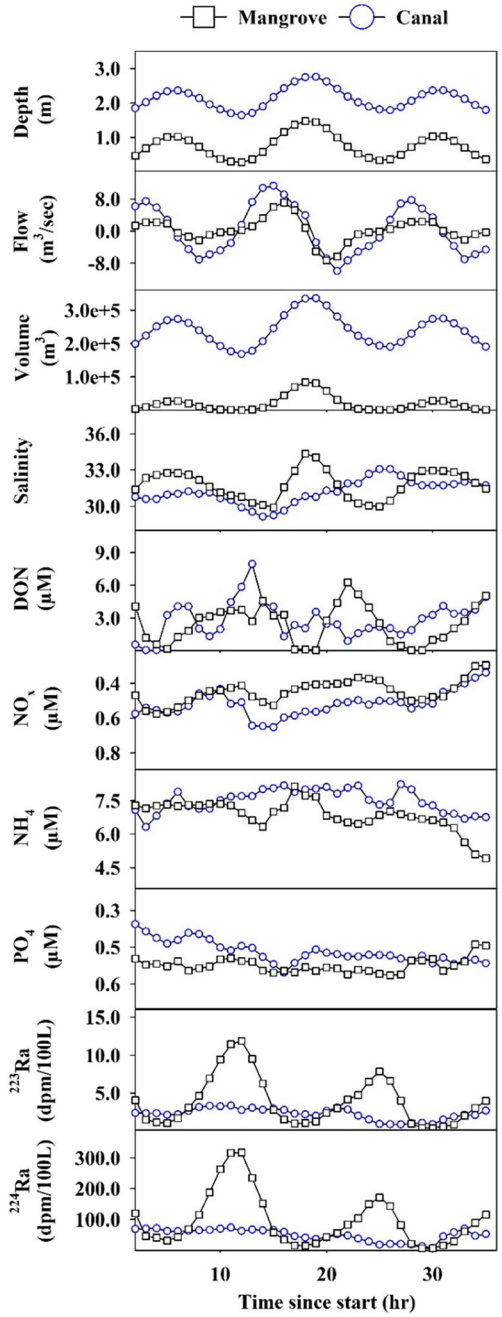

Fig. 2 Time series surface water observations of water chemistry at both sites (mangrove and canal) of Yamba. Time series experiment started on 14 June 2018 04:00 h

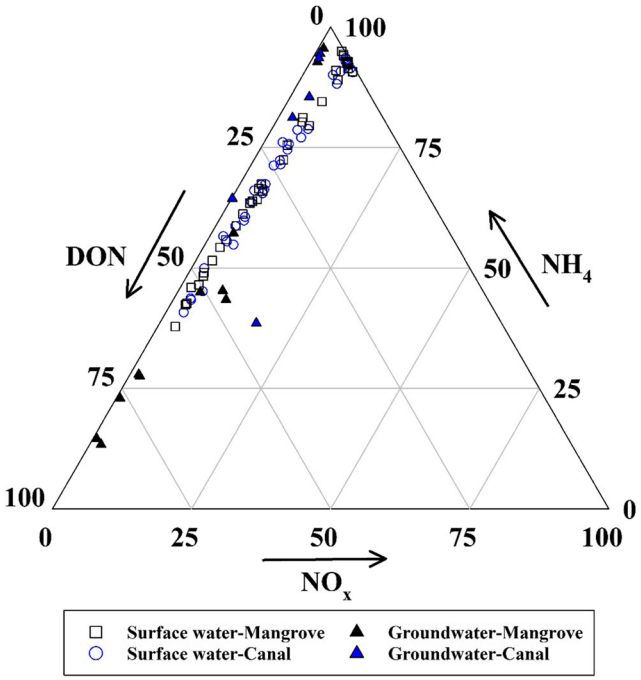

Fig. 3 The relative contribution of the different nitrogen species in surface water and groundwater. NH_4 was the dominant nitrogen species surface and groundwater at both sites, whereas DON dominated mangrove groundwater

with low activity ocean water at high tide. We highlight, however, that the mass balance model is based on radium fluxes rather than activities. Mean radium isotope concentrations (4.0 ± 3.6 dpm/100 L for ^{223}Ra and 99.4 ± 96.3 dpm/100 L for ^{224}Ra) in the mangrove creek were nearly double those observed in the canal (2.2 ± 1.0 dpm/100 L for ^{223}Ra and 51.0 ± 25.9 dpm/100 L for ^{224}Ra respectively).

Groundwater Observations

Groundwater ^{223}Ra and ^{224}Ra concentrations were higher than surface water radium concentrations at both sites (Table 2 and Fig. 2). Groundwater ^{223}Ra and ^{224}Ra had no clear relationship with salinity. Canal groundwater had greater mean concentrations of NH_4 and TDN than mangrove groundwater (Table 2), and an 8-fold higher DIN:DIP ratio. The TDN pool in mangrove groundwater consisted of 52.7% DON and 47.3% DIN (3.1% nitrate + nitrite and 44.2% ammonium) while canal groundwater consisted of 19.5% DON and 80.5% DIN (4.2% nitrate + nitrite and 76.3% ammonium) (Fig. 3).

Radium Mass Balance to Estimate Groundwater Exchange

Short-lived radium isotope (^{223}Ra and ^{224}Ra) mass balances were used to calculate the net flux of groundwater exchange. Figure 4 shows radium isotope (^{223}Ra and

Table 2 Groundwater observations from the mangrove and canal intertidal area

	ID	pH	Salinity	NO_x	NH_4	PO_4	TDN	^{223}Ra	^{224}Ra
				μmol L^{-1}	μmol L^{-1}	μmol L^{-1}	μmol L^{-1}	(dpm/100 L)	(dpm/100 L)
Mangrove	GW M1	7.4	33.5	0.5	57.2	1.7	36.8	52.72	1802.5
	GW M2	7.1	33.9	0.6	46.1	3.7	38.3	18.01	751.1
	GW M3	6.8	36.3	0.4	2.7	16.3	20.5	40.70	1916.8
	GW M4	7.4	34.7	0.5	7.6	0.6	13.4	39.66	730.7
	GW M5	6.7	24.5	1.5	8.7	0.5	19.2	46.36	777.5
	GW M6	6.8	31.1	0.4	9.6	0.6	65.8	49.00	948.5
	GW M7	6.4	3.9	1.0	14.9	1.8	54.3	21.85	524.9
	GW M8	6.5	16.1	0.4	12.2	0.4	53.3	48.88	1066.4
	GW M9	7.2	33.6	2.0	9.3	0.4	21.4	32.73	706.9
	GW M10	6.6	32.8	0.7	8.3	0.5	18.5	72.54	1185.8
	GW M11	7.0	32.5	0.4	7.7	0.5	27.6	62.8	1008.7
	Avg. ± SE	6.9 ± 0.1	28.4 ± 3.0	0.8 ± 0.2	16.8 ± 5.3	2.5 ± 1.4	33.5 ± 5.3	44.1 ± 4.9	1038.2 ± 135
Canal	GW C1	6.2	6.2	20.0	44.5	0.1	115.4	14.2	338.8
	GW C2	6.6	29.0	0.5	62.7	0.7	43.0	20.6	441.9
	GW C3	6.6	0.9	0.2	135.0	0.8	209.4	20.5	894.9
	GW C4	6.9	27.0	0.4	35.1	0.4	21.2	29.6	1023.1
	GW C5	7.4	27.6	1.1	36.5	0.4	44.9	33.9	886.3
	GW C6	7.5	26.7	1.3	33.3	0.8	38.9	40.5	1042.4
	Avg. ± SE	6.8 ± 0.2	19.5 ± 5.1	4.0 ± 3.2	57.9 ± 16.0	0.5 ± 0.1	78.8 ± 29.3	26.5 ± 4.0	771.2 ± 124

^{224}Ra) fluxes with 1-h time intervals over 36 h. Diffusion from sediments and radioactive decay were the smallest radium source and sink at both sites (Table 3 and Fig. 4). The ^{223}Ra and ^{224}Ra fluxes integrated over three complete tidal cycles revealed groundwater exchange rates based on ^{223}Ra and ^{224}Ra at 1.3 ± 0.4 and 3.4 ± 0.9 cm day^{-1}, respectively, in the mangrove creek. At the canal estate, groundwater exchange rates were ~2-fold higher (3.4 ± 0.9 for ^{223}Ra and 5.4 ± 4.6 cm day^{-1} for ^{224}Ra) in the canal over a 36-h time scale.

Nutrient Fluxes via SGD and Lateral Exchange

The net lateral TDN fluxes from the canal estate were 2-fold higher than the mangrove creek (Table 4 and Fig. 5). The mangrove creek was a source of DON to the adjacent estuary (2.8 mmol m^{-2} day^{-1}), and the canal showed a net import of DON (0.9 mmol m^{-2} day^{-1}). Net lateral fluxes of NO_x weighted over water surface area did not show a significant difference between systems, while net fluxes of NH_4 were higher in the mangrove creek (Table 4).

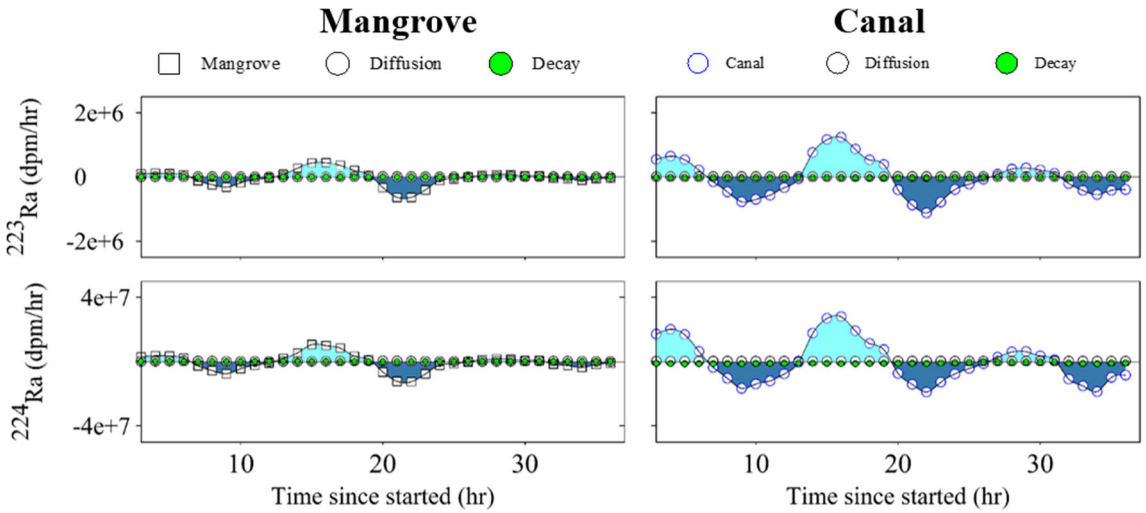

Fig. 4 Hourly radium isotope (^{223}Ra and ^{224}Ra) fluxes over 36 h, integrated to quantify groundwater exchange rates

Table 3 ^{223}Ra and ^{224}Ra mass balance terms and radium-derived groundwater exchange rates integrated over 36 h for the mangrove and canal sites

	Units	Mangrove	Canal
^{223}Ra			
Incoming tide	dpm day^{-1}	$4.5 \times 10^6 \pm 5.5 \times 10^5$	$1.3 \times 10^7 \pm 1.5 \times 10^6$
Outgoing tide	dpm day^{-1}	$4.3 \times 10^6 \pm 6.1 \times 10^5$	$1.1 \times 10^7 \pm 1.3 \times 10^6$
Diffusion	dpm day^{-1}	$9.0 \times 10^4 \pm 6.2 \times 10^3$	$2.5 \times 10^5 \pm 1.5 \times 10^4$
Decay	dpm day^{-1}	$1.7 \times 10^4 \pm 2.3 \times 10^3$	$3.3 \times 10^5 \pm 3.8 \times 10^4$
Missing (groundwater)	dpm day^{-1}	$2.8 \times 10^5 \pm 6.7 \times 10^4$	$1.2 \times 10^6 \pm 2.5 \times 10^5$
Groundwater endmember	dpm/100 L	41.0 ± 8.8	24.6 ± 4.7
Groundwater exchange rate (total)	m^3 day^{-1}	7.0×10^2	4.8×10^3
Groundwater exchange rate (per unit area)	cm day^{-1}	1.3 ± 0.4	3.4 ± 0.9
^{224}Ra			
Incoming tide	dpm day^{-1}	$1.1 \times 10^8 \pm 4.4 \times 10^7$	$3.1 \times 10^8 \pm 1.3 \times 10^8$
Outgoing tide	dpm day^{-1}	$9.4 \times 10^7 \pm 4.8 \times 10^7$	$2.4 \times 10^8 \pm 9.2 \times 10^7$
Diffusion	dpm day^{-1}	$3.5 \times 10^6 \pm 7.4 \times 10^5$	$9.7 \times 10^6 \pm 1.7 \times 10^6$
Decay	dpm day^{-1}	$1.2 \times 10^6 \pm 5.5 \times 10^5$	$2.4 \times 10^7 \pm 9.3 \times 10^6$
Missing (groundwater)	dpm day^{-1}	$1.4 \times 10^7 \pm 1.2 \times 10^7$	$5.6 \times 10^7 \pm 3.9 \times 10^7$
Groundwater endmember	dpm/100 L	$9.6 \times 10^2 \pm 6.6 \times 10^2$	$7.2 \times 10^2 \pm 3.5 \times 10^2$
Groundwater exchange rate (total)	m^3 day^{-1}	1.5×10^3	7.7×10^3
Groundwater exchange rate (per unit area)	cm day^{-1}	2.8 ± 3.0	5.4 ± 4.6

Mangrove groundwater released 5-fold less TDN to the surface water than the canal estate (Table 4). SGD-derived NO_x and NH_4 loads were ~5-fold and ~7-fold higher in the canal than the mangrove. SGD-derived TDN loads were estimated to be 0.7 and 3.4 mmol m^{-2} day^{-1} in mangrove and canal respectively.

Discussion

Groundwater Exchange Rates

Our radium isotope mass balance model revealed relatively low groundwater exchange rates at both sites ranging from 1.3 to 5.4 cm day^{-1} (Table 3). Radium-derived SGDs were twice as high in the canal than in the mangrove. While a number of recent investigations have quantified this process in mangrove creeks (Sadat-Noori et al. 2017; Taillardat et al. 2019; Tait et al. 2017), very little research exists on quantifying groundwater flows in residential canals and drains to assess the impact of natural system replacement (Macklin et al. 2014; Webb et al. 2019). Here, we compared two adjacent systems to gain insight into how artificial canals may differ from mangroves.

Groundwater exchange rates range from 2.1 to 35.5 cm day^{-1} in Australian tropical, subtropical, and temperate tidal mangrove creeks (Tait et al. 2016). In a nearby subtropical estuary, groundwater exchange rates were 13.6–27.8 cm day^{-1} (Sadat-Noori et al. 2017). There is limited information on how artificial canals affect groundwater flows.

Table 4 Estimated surface water nutrient fluxes and groundwater-derived nutrient fluxes at mangrove and canal. Positive fluxes represent an input into the mangrove or canal, while negative fluxes represent a flux out of the mangrove or canal

	Mangrove						Canal				
	Units	NO_x	NH_4	DON	PO_4	TDN	NO_x	NH_4	DON	PO_4	TDN
Incoming tide	mol day^{-1}	122.1	1756.0	375.4	130.6	2253.0	334.5	4366.7	1298.6	273.9	5999.7
Outgoing tide	mol day^{-1}	−76.2	−1209.9	−524.8	−97.0	−1810.0	−209.8	−3311.8	−1168.4	−211.4	−4690.1
Net lateral flux	mol day^{-1}	46.0	546.8	−149.0	33.7	443.8	124.7	1054.8	130.1	62.5	1309.6
Net lateral flux	mmol m^{-2} of water area day^{-1}	0.9	10.3	−2.8	0.6	8.4	0.9	7.3	0.9	0.4	9.1
Groundwater-derived flux	mmol m^{-2} of water area day^{-1}	0.02	0.3	0.4	0.1	0.7	0.2	2.5	0.7	0.02	3.4

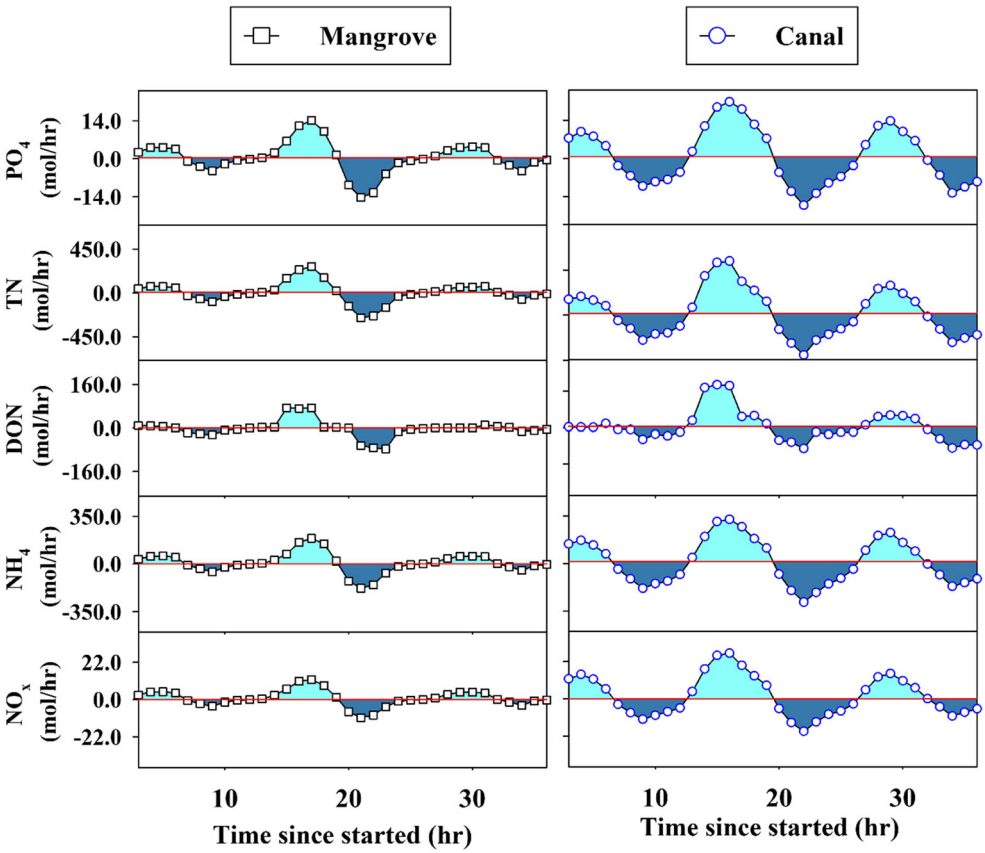

Fig. 5 Surface water dissolved nutrient fluxes at mangrove and canal sites with 1 h time interval over 36 h. The fluxes were integrated to quantify net lateral exports into the adjacent estuary

A man-made (~ 5 m) deep canal (C-54 Canal, USA) had 8-fold higher groundwater discharge (2.4×10^5–3.0×10^4 m^3 day^{-1}) than nearby shallow (> 1 m) creeks (North Prong, USA) (Santos et al. 2010). Similarly, the 2-m deep canal here has a ~ 2-fold higher groundwater exchange rate than the nearby shallow (< 1 m) mangrove creek. C-54 canal was built in the subtropical USA by draining freshwater coastal wetlands. Soil along the C-54 canal was a mix of sand, silt, and clay similar to our mangrove system, but the system is not tidal. The tidal range is relatively higher in Yamba (15 cm in USA versus 120 cm in Australia), enhancing the contribution of tidal pumping as a driver of SGD. The exchange rate in man-made canals in the subtropical Dux Creek canal was estimated at 3.1 ± 1.5 cm day^{-1}, consistent with our estimates (Davis et al. 2020).

In radium mass balance models, the major source of uncertainty is often related to assigning an endmember value to groundwater (Burnett et al. 2007; Cerdà-Domènech et al. 2017). The concentration of radium in groundwater can vary substantially over small spatial scales (Schmidt et al. 2010). Our endmember sample size ($n = 11$ in the mangrove and 6 in the canal) allowed us to minimize those uncertainties to 15.1 and 16.1%, respectively (Sadat-Noori et al. 2015). If we use the median (46.4 and 948.5 dpm/100 L for ^{223}Ra and ^{224}Ra in the mangrove, 25.1 and 890.6 dpm/100 L for ^{223}Ra and ^{224}Ra in the canal) rather than the mean (44.1 and 1038.2 dpm/100 L in the mangrove, 26.5 and 771.2 dpm/100 L in the canal) radium concentration in groundwater as the endmember, the final SGD estimates would reduce by around 5% in both mangrove and canal systems. Our groundwater samples had a range in salinity from 0.9 to 34.7. Radium is known to desorb from sediments at salinities greater than 5 (Peterson et al. 2008). If all groundwater samples with salinity < 5 are excluded from the mean, the final SGD rates would change by 5 and 6% in the mangrove creek and canal, respectively. From our surface water salinity observations and the local geomorphology, it is clear that fresh groundwater cannot be a major source of radium to the mangrove or canal.

The driving forces of groundwater flow depend on precipitation, tides-waves, geology, vegetation, land use, and interaction with beach morphology (Robinson et al. 2006; Rufí-Salís et al. 2019; Taniguchi et al. 2019). Both sites receive runoff from urban land use following rain events; however, no runoff was observed during our experiments simplifying the interpretation of our observations. Runoff from urban land use contains mainly NO_x (Taylor et al. 2005), whereas mangrove systems are often enriched in ammonium (Singh et al. 2005). Tidal range and waves at both sites were similar (1.2 m) (Table 1). Because both sites have similar geographic and hydrological settings, the morphological differences, such as grain size distributions, are likely the predominant factors that define each system.

The canal intertidal zone had course sands, while the mangrove intertidal zone had fine-grain muds abundant with crab burrows (Fig. 6). The transmission of surface water through the burrows depends upon the sediment grain size and the density of crab burrows (Schwendenman et al. 2006; Xiao et al. 2019b; Xin et al. 2009). Crab burrows modify physical characteristics of the sediment (Ridd 1996). Schwendenman et al. (2006) found sediment permeability was lower (< 0.1 m day^{-1}) in the clay-rich and crab burrow-free mud layer, whereas fine sand strata permeability ranged from 0.7 to 1.8 m day^{-1} in a crab burrow-rich mangrove creek. Even though crab burrows should enhance groundwater flows, we observed lower exchange in the mangrove. At our mangrove site, recirculated seawater also infiltrates through low permeability mangrove muds, which may explain relatively lower groundwater exchange rates at this site. Therefore, we suspect difference between the mangrove and canal may be primarily attributed to the sediment type and geomorphology.

We also suspect steeper banks in the canal may promote greater groundwater exchange rates (bank slope canal 21% versus mangrove 8%). Man-made land modification have an impact on bank slope and its stability (Jiao 2000) and therefore may alter hydraulic conditions (e.g., inland hydraulic head and slope break drainage) and increase the groundwater flow to the sea (Jiao 2000; Zhang et al. 2017). Numerical simulations have also indicated that increases in the beach slope can increase groundwater flow and modify drainage characteristic in the intertidal zone (Li et al. 2008).

Nutrient Groundwater and Lateral Loads

Regional and global-scale nitrogen budgets indicate that most of the dissolved N in anthropogenic landscapes are processed within estuaries and do not reach the coastal ocean (Meter et al. 2016; Wang et al. 2019). Intertidal wetlands are well-known to attenuate nitrogen pollution along estuarine conduits (Alongi 2002; Wadnerkar et al. 2019; Wang et al. 2019), but may still export nitrogen that fuels coastal food webs (Santos et al. 2014; Smith 2006; Wang et al. 2019). Are mangroves sources or sinks of nitrogen to the coastal ocean, and how do they compare with canals? Our simultaneous observations allow for a direct comparison between a mangrove and a canal.

This study is consistent with other observations in non-contaminated mangrove creeks (Tait et al. 2017). TDN was imported from the nearby estuary into both the mangrove and canal at similar rates (8.4 ± 1.1 and 9.1 ± 1.1 mmol m^{-2} day^{-1}, respectively, Table 4). These estimates are in the middle of estuarine-derived TDN import estimates from the dry tropics (2 mmol m^{-2} day^{-1}) to the subtropics (15 mmol m^{-2} day^{-1}) (Tait et al. 2017). PO_4 import was 0.6 ± 0.1 at the mangrove and 0.4 ± 0.1 mmol m^{-2} day^{-1} at the canal which is equivalent to a mangrove subtropical creek (Gleeson et al. 2013).

Groundwater-derived TDN export to surface water in the mangrove and canal was 0.7 ± 0.1 and 3.4 ± 0.7 mmol m^{-2} day^{-1}, lower than earlier observations in an intertidal mangrove creek at temperate Barwons Head, Australia (TDN ~ 3 mmol m^{-2} day^{-1}) but higher than dry tropical Toms Creek (0.5 mmol m^{-2} day^{-1}) (Tait et al. 2017) where no obvious freshwater inputs were observed. In the previous cases, differences between systems seem to be explained by different climatic conditions like dry tropical and temperate conditions. In the sandy sediments of the highly modified Tolo Harbor, Hong Kong, groundwater-derived DIN fluxes were 0.6–1.4 mmol m^{-2} day^{-1} (Luo et al. 2014) which is consistent with our groundwater-derived DIN fluxes in the canal estate (Table 5). Similarly, the salt marshes with fine-grained interbedded sand of South Carolina have similar DIN fluxes (2.4 mmol m^{-2} day^{-1}) (Krest et al. 2000). Here, groundwater exchange in the mangrove creek released ~ 5-

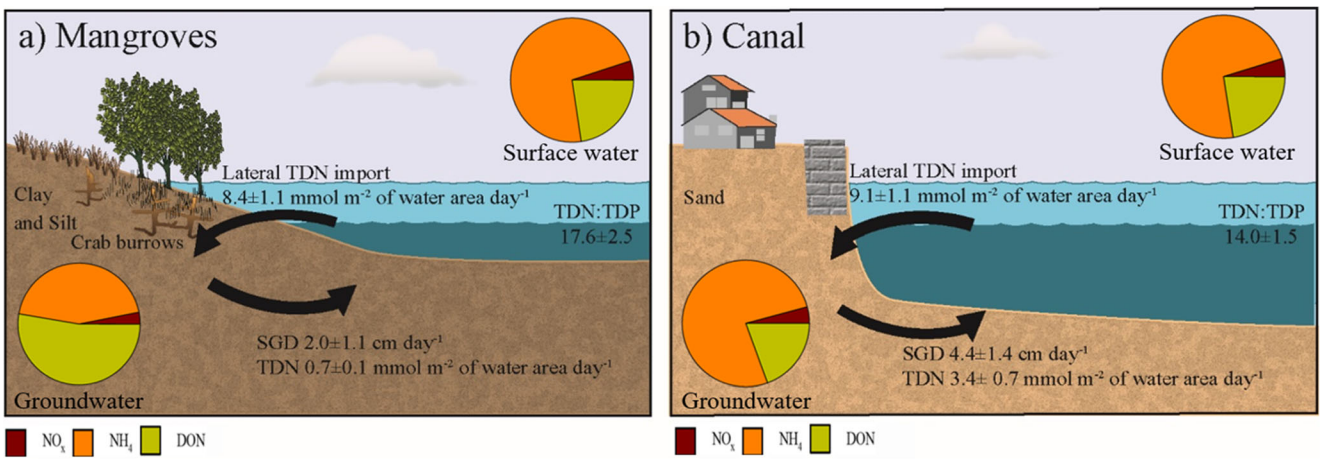

Fig. 6 Conceptual model illustrating groundwater exchange rates (SGD) and groundwater-derived total dissolved nitrogen export in mangrove and canal site of Yamba (modified from Davis et al. 2020)

Table 5 Comparison of groundwater fluxes from coastal wetlands and canals from prior studies

Site	Ecosystem description	Sediments	Habitat	Groundwater exchange rate (cm day^{-1})	Groundwater-derived TDN (mmol m^{-2} day^{-1})	Reference
Jacobs Well	Subtropical tidal mangrove creek	Silt and clay	Mangrove	7.3–25.7	9.0	Webb et al. (2019) and Tait et al. (2017)
Evans River	Subtropical tidal mangrove creek	Silt and clay	Mangrove	8.4 ± 1.8		Webb et al. (2019)
Barwon Heads	Subtropical tidal mangrove creek	Silt and clay	Saltmarsh and mangrove	3.7 ± 2.4		Webb et al. (2019)
Kangaroo Island	Subtropical tidal mangrove creek	Silt and clay	Mangrove	0.3	26.6	Gleeson et al. (2013)
Kooragang Island	Temperate tidal mangrove creek	Silt and clay	Mangrove	14.0 ± 6.3	21.3 ± 5.5	Sadat-Noori and Glamore (2019)
Watson Inlet	Temperate tidal mangrove creek	Silt and clay	Mangrove and saltmarsh	27.0		Faber et al. (2014)
Chinaman Inlet, Australia	Temperate tidal mangrove creek	Silt and clay	Mangrove and saltmarsh	6.7		Faber et al. (2014)
Can gio mangrove creek	Temperate tidal mangrove creek	Silt, clay, and sand	Mangrove and saltmarsh	3.1–7.1		Taillardat et al. (2018)
Hunter River	Subtropical mangrove estuary	Silt and clay	Saltmarsh and Mangrove	14.7 ± 2.9		Webb et al. (2019)
Korogoro Creek	Subtropical mangrove estuary	Sand, Silt, and clay	Mangrove and saltmarsh	35		Webb et al. (2019)
Korogoro Creek	Subtropical mangrove estuary	Sand, Silt, and clay	Mangrove and saltmarsh	18–84		Sadat-Noori et al. (2015)
Coffs Creek	Subtropical mangrove estuary	Sand, silt, and clay	Mangrove	13.6–27.8		Sadat-Noori et al. (2017)
Shark River Estuary, USA	Subtropical mangrove estuary	Mangrove soil (silt and clay)	Mangrove	2.1		Smith et al. (2016)
Wanquan River Estuary, China	Tropical mangrove estuary	Sand, silt, and gravel	Mangrove	0.5		Su et al. (2011)
Sadgroves Creek	Tropical mangrove estuary	Silt and clay	Mangrove	6.1–15.1	4.0	Tait et al. (2017)
Coral Creek	Tropical mangrove estuary	Silt and clay	Mangrove	24.5–29.7	2.0	Tait et al. (2017)
Tom's Creek	Tropical mangrove estuary	Silt and clay	Mangrove	1.8–7.5	1.0	Tait et al. (2017)
Dunns Creek	Subtropical mangrove estuary	Silt and clay	Mangrove	5.3–8.7	6.0	Tait et al. (2017)
Barwan Creek	Temperate mangrove estuary	Silt and clay	Mangrove	1.2–1.5	0.8	Tait et al. (2017)
Sepetiba Bay, Brazil	Subtropical mangrove patched bay	Mangrove peat and clay	Mangrove	8		Sanders et al. (2012)
Bamen Bay, China	Tropical mangrove patched bay	Sand, silt, and gravel	Mangrove and corals	1.5		Su et al. (2011)
Hainan Island, China	Subtropical mangrove swamp	Silt and clay	Mangrove	0.086–50		Xia and Li (2012)
Daya Bay, China	Subtropical mangrove swamp	Silt and clay?	Mangrove and saltmarsh	0.06–3.2		Xiao et al. (2019a)
Cocoa Creek	Tropical mangrove swamp	Mangrove sediments (silt and clay)	Mangrove and saltmarsh	2.4		Susilo et al. (2005)
Laoye Lagoon, China	Tropical mangrove lagoon	Sand	Mangrove and saltmarsh	9.4		Wang and Du (2016)

Table 5 (continued)

Site	Ecosystem description	Sediments	Habitat	Groundwater exchange rate (cm day^{-1})	Groundwater-derived TDN (mmol m^{-2} day^{-1})	Reference
Xiaohai Lagoon, China	Tropical mangrove lagoon	Sand	Mangrove and saltmarsh	4.1		Wang and Du (2016)
C-25, Indian River Lagoon, USA	Subtropical canal	Sand and clay		3–25		Peterson et al. (2010)
Hood Canal	Temperate canal (natural waterway)			85		Swarzenski et al. (2007)
Bribie Island	Subtropical canal	Sand	Mangrove and saltmarsh	3.1 ± 1.5		Davis et al. (2020)
Yamba (canal)	Subtropical canal	Sand		4.4 ± 1.4	3.4 ± 0.7	This study
Yamba (mangrove)	Subtropical tidal mangrove creek	Silt and clay	Mangrove	2.0 ± 1.1	0.7 ± 0.0	This study

fold less TDN to surface waters than canal. At the mangrove site, groundwater was a net source of DON (Table 5) and positively correlated with radium isotopes.

There are three major nitrogen sequestrations, loss, or uptake processes in mangrove systems: (1) nitrogen uptake by plants, microbes, and microalgae in surface and subsurface waters, (2) burial in sediments, and (3) denitrification (Alongi 1996; Taillardat et al. 2019; Wadnerkar et al. 2019). Organic material, such as litter fall, may be buried by crabs, increasing ammonification and the resulting release of inorganic nutrients that are bioavailable for vegetation and mangrove uptake (Feller et al. 2003). Ammonium is preferentially assimilated by mangrove plants and phytoplankton and incorporated by the large belowground root network (Balk et al. 2015; Reef et al. 2010). Burial in mangrove sediments can be a significant pathway for particulate nitrogen loss from estuarine systems (Kristensen et al. 1998; Rivera-Monroy et al. 1995; Sanders et al. 2014). For instance, in a tropical mangrove, nitrogen accumulated in sediments of vegetated areas at greater rates than non-vegetated areas (1.9 and 1.2 kg N km^{-2} day^{-1}, respectively) (Kristensen et al. 1998).

Human-impacted mangroves in Southeast China have been identified as important sites of denitrification where nitrate removal takes place from porewater producing N_2O and N_2 (Wang et al. 2019). Denitrification was found to be the leading pathway for nitrogen loss in a subtropical mangrove in China (~90%) (Xiao et al. 2018). Further, denitrification rates in vegetated sediments were 3-fold higher than non-vegetated intertidal zones of a southeast Asian mangrove forest (0.6 kg N km^{-2} day^{-1} in vegetated sediments and 0.2 kg N km^{-2} day^{-1} in un-vegetated sediments) (Kristensen et al. 1998).

Sand beach ecosystems can also process, re-mineralize, and accumulate dissolved nutrients, which can be transported via groundwater to nearshore waters and available for primary producers (Dugan et al. 2011). Normally, permeable sands on the beach have low organic content but high organic matter turnover (Dugan et al. 2011). In this study, the mangrove released 5-fold less (TDN) than the canal estate (Table 4), suggesting groundwater-derived nutrients were flushed/recirculated in sands of the canal system.

Conclusions

Groundwater exchange and associated nutrient fluxes were concurrently estimated using short-lived radium isotopes (^{223}Ra and ^{224}Ra) at a natural mangrove and artificial canal site. Overall, the canal had 2-fold higher groundwater exchange rates than nearby mangrove creek and released 5-fold more groundwater-derived dissolved nitrogen into surface waters. Both the mangrove and canal surface waters

imported nutrients from the nearby estuary, indicating that mangroves are more efficient at retaining TDN. Therefore, canal estate development not only drive losses of estuarine ecosystem services, but also modify groundwater flows and the nitrogen cycle in coastal areas. Our results highlight how preserving mangroves may offer major benefits to coastal water quality by retaining nitrogen rather than exporting to the coastal ocean.

Acknowledgments The authors would like to thank Sara Lock who performed the nutrient analysis.

Funding Information Funding was provided by the Australian Research Council (FT170100327; LE170100007). Bayartungalag Batsaikhan's contribution was supported by an Australian Endeavour Fellowship covering her work in Australia.

References

Adame, M.F., M.E. Roberts, D.P. Hamilton, C.E. Ndehedehe, V. Reis, J. Lu, M. Griffiths, G. Curwen, and M. Ronan. 2019. Tropical coastal wetlands ameliorate nitrogen export during floods. *Frontiers in Marine Science* 6: 671.

Alongi, D.M. 1996. The dynamics of benthic nutrient pools and fluxes in tropical mangrove forests. *Journal of Marine Research* 54 (1): 123–148.

Alongi, D.M. 2002. Present state and future of the world's mangrove forests. *Environmental Conservation* 29 (3): 331–349.

Alongi, D., L. Trott, G. Wattayakorn, and B. Clough. 2002. Belowground nitrogen cycling in relation to net canopy production in mangrove forests of southern Thailand. *Marine Biology* 140: 855–864.

Atkins, M.L., I.R. Santos, S. Ruiz-Halpern, and D.T. Maher. 2013. Carbon dioxide dynamics driven by groundwater discharge in a coastal floodplain creek. *Journal of Hydrology* 493: 30–42.

Balfour, A., Bost, M., Cook, C., Couper, L., Ellis, P., English, M., Gooding, E., Housego, R., Kaufmann, R., Posey, S., 2012. Water Quality in the Pine Knoll shores Residential Canal System.

Balk, M., A.M. Laverman, J.A. Keuskamp, and H.J. Laanbroek. 2015. Nitrate ammonification in mangrove soils: a hidden source of nitrite? *Frontiers in Microbiology* 6: 166.

Benfer, N.P., B.A. King, C.J. Lemckert, and S. Zigic. 2010. Modeling the effect of flow structure selection on residence time in an artificial canal system: case study. *Journal of Waterway, Port, Coastal, and Ocean Engineering* 136 (2): 91–96.

BOM, 2017. Climate Statistics for Australian Locations. Coffs Harbour Meteorological Office Bureau of Meteorology.

BOM, 2019 Climate Statistics for Australian Locations.

Bureau of Statistics, A., 2017.

Burnett, W.C., and H. Dulaiova. 2003. Estimating the dynamics of groundwater input into the coastal zone via continuous radon-222 measurements. *Journal of Environmental Radioactivity* 69 (1-2): 21–35.

Burnett, W., P. Aggarwal, A. Aureli, H. Bokuniewicz, J. Cable, M. Charette, E. Kontar, S. Krupa, K. Kulkarni, and A. Loveless. 2006. Quantifying submarine groundwater discharge in the coastal zone via multiple methods. *Science of the Total Environment* 367 (2-3): 498–543.

Burnett, W.C., I.R. Santos, Y. Weinstein, P.W. Swarzenski, and B. Herut. 2007. Remaining uncertainties in the use of Rn-222 as a quantitative tracer of submarine groundwater discharge. *IAHS Publication* 312: 109.

Burnett, W.C., R.N. Peterson, I.R. Santos, and R.W. Hicks. 2010. Use of automated radon measurements for rapid assessment of groundwater flow into Florida streams. *Journal of Hydrology* 380 (3-4): 298–304.

Cardwell, R.D., E.P. Richey, and R.E. Nece. 1980. Fish, flushing, and water quality: their roles in marina design, Coastal Zone'80. *ASCE*: 84–103.

Cerdà-Domènech, M., V. Rodellas, A. Folch, and J. Garcia-Orellana. 2017. Constraining the temporal variations of Ra isotopes and Rn in the groundwater end-member: implications for derived SGD estimates. *Science of the Total Environment* 595: 849–857.

Chen, X., F. Zhang, Y. Lao, X. Wang, J. Du, and I.R. Santos. 2018. Submarine groundwater discharge-derived carbon fluxes in mangroves: an important component of blue carbon budgets? *Journal of Geophysical Research: Oceans* 123 (9): 6962–6979.

Choi, J., and J.W. Harvey. 2000. Quantifying time-varying ground-water discharge and recharge in wetlands of the northern Florida Everglades. *Wetlands* 20 (3): 500–511.

Cook, S.S., J.L. Roberts, G.M. Hallegraeff, and A. McMinn. 2007. Impact of canal development on intertidal microalgal productivity: comparative assessment of Patterson Lakes and Ralphs Bay, South East Australia. *Journal of Coastal Conservation* 11 (3): 171–181.

Davis, K., I.R. Santos, A.K. Perkins, J.R. Webb, and J. Gleeson. 2020. Altered groundwater discharge and associated carbon fluxes in a wetland-drained coastal canal. *Estuarine, Coastal and Shelf Science* 235: 106567.

De Weys, J., I.R. Santos, and B.D. Eyre. 2011. Linking groundwater discharge to severe estuarine acidification during a flood in a modified wetland. *Environmental science technology* 45 (8): 3310–3316.

Dugan, J.E., D.M. Hubbard, H.M. Page, and J.P. Schimel. 2011. Marine macrophyte wrack inputs and dissolved nutrients in beach sands. *Estuaries and Coasts* 34 (4): 839–850.

Faber, P.A., V. Evrard, R.J. Woodland, I.C. Cartwright, and P.L. Cook. 2014. Pore-water exchange driven by tidal pumping causes alkalinity export in two intertidal inlets. *Limnology and Oceanography* 59 (5): 1749–1763.

Feller, I.C., D.F. Whigham, K.L. McKee, and C.E. Lovelock. 2003. Nitrogen limitation of growth and nutrient dynamics in a disturbed mangrove forest, Indian River Lagoon, Florida. *Oecologia* 134 (3): 405–414.

Garcia-Orellana, J., J. Cochran, H. Bokuniewicz, S. Yang, and A.J. Beck. 2010. Time-series sampling of 223Ra and 224Ra at the inlet to Great South Bay (New York): a strategy for characterizing the dominant terms in the Ra budget of the bay. *Journal of Environmental Radioactivity* 101 (7): 582–588.

Garcia-Solsona, E., J. Garcia-Orellana, P. Masqué, and H. Dulaiova. 2008. Uncertainties associated with 223Ra and 224Ra measurements in water via a Delayed Coincidence Counter (RaDeCC). *Marine Chemistry* 109 (3-4): 198–219.

Gedan, K.B., M.L. Kirwan, E. Wolanski, E.B. Barbier, and B.R. Silliman. 2011. The present and future role of coastal wetland vegetation in protecting shorelines: answering recent challenges to the paradigm. *Climatic Change* 106 (1): 7–29.

Gleeson, J., I.R. Santos, D.T. Maher, and L. Golsby-Smith. 2013. Groundwater–surface water exchange in a mangrove tidal creek: evidence from natural geochemical tracers and implications for nutrient budgets. *Marine Chemistry* 156: 27–37.

Harvard, U. O., 2007. A summary of error propagation. http://ipl.physics.harvard.edu/wp-uploads/2013/2003/PS2013_Error_Propagation_sp2013.pdf.

Harvey, J.W., J.E. Saiers, and J.T. Newlin. 2005. Solute transport and storage mechanisms in wetlands of the Everglades, south Florida. *Water Resources Research* 41: 5009.

Jiao, J.J. 2000. Modification of regional groundwater regimes by land reclamation. *Journal of Hong Kong Geologist* 6: 29–36.

Krest, J.M., W. Moore, L. Gardner, and J. Morris. 2000. Marsh nutrient export supplied by groundwater discharge: evidence from radium measurements. *Global Biogeochemical Cycles* 14 (1): 167–176.

Kristensen, E. 2008. Mangrove crabs as ecosystem engineers; with emphasis on sediment processes. *Journal of Sea Research* 59 (1-2): 30–43.

Kristensen, E., and D.M. Alongi. 2006. Control by fiddler crabs (Uca vocans) and plant roots (Avicennia marina) on carbon, iron, and sulfur biogeochemistry in mangrove sediment. *Limnology and Oceanography* 51 (4): 1557–1571.

Kristensen, E., M.H. Jensen, G.T. Banta, K. Hansen, M. Holmer, and G.M. King. 1998. Transformation and transport of inorganic nitrogen in sediments of a southeast Asian mangrove forest. *Aquatic Microbial Ecology* 15: 165–175.

Leung, J.Y., Q. Cai, and N.F. Tam. 2016. Comparing subsurface flow constructed wetlands with mangrove plants and freshwater wetland plants for removing nutrients and toxic pollutants. *Ecological Engineering* 95: 129–137.

Li, H., M.C. Boufadel, and J.W. Weaver. 2008. Tide-induced seawater–groundwater circulation in shallow beach aquifers. *Journal of Hydrology* 352 (1-2): 211–224.

Luo, X., J.J. Jiao, W. Moore, and C.M. Lee. 2014. Submarine groundwater discharge estimation in an urbanized embayment in Hong Kong via short-lived radium isotopes and its implication of nutrient loadings and primary production. *Marine Pollution Bulletin* 82 (1-2): 144–154.

Macintosh, D.J., and E.C. Ashton. 2002. *A review of mangrove biodiversity conservation and management. Centre for tropical ecosystems research*. Denmark: University of Aarhus.

Macklin, P.A., D.T. Maher, and I.R. Santos. 2014. Estuarine canal estate waters: hotspots of CO2 outgassing driven by enhanced groundwater discharge? *Marine Chemistry* 167: 82–92.

Macklin, P.A., I.R. Santos, D.T. Maher, and C.J. Sanders. 2017. Mapping short-lived radium isotopes in estuarine residential canals (Gold Coast, Australia). *Journal of Radioanalytical and Nuclear Chemistry* 313 (2): 409–418.

Macnae, W. 1969. A General Account of the Fauna and Flora of Mangrove Swamps and Forests in the Indo-West-Pacific Region. In *Advances in Marine Biology*, ed. F.S. Russell and M. Yonge, 73–270. Academic Press.

Meter, K.J.V., N.B. Basu, J.J. Veenstra, and C.L. Burras. 2016. The nitrogen legacy: emerging evidence of nitrogen accumulation in anthropogenic landscapes. *Environmental Research Letters* 11 (3): 035014.

Moore, W.S. 2010. A reevaluation of submarine groundwater discharge along the southeastern coast of North America. *Global Biochemical Cycles* 24: 4005.

Moore, W.S., and R. Arnold. 1996. Measurement of 223Ra and 224Ra in coastal waters using a delayed coincidence counter. *Journal of Geophysical Research: Oceans* 101 (C1): 1321–1329.

Moore, W.S., Blanton, J.O., Joye, S.B 2006. Estimates of flushing times, submarine groundwater discharge, and nutrient fluxes to Okatee Estuary, South Carolina. 111.

Morton, R. 1989. Hydrology and fish fauna of canal developments in an intensively modified Australian estuary. *Estuarine, Coastal and Shelf Science* 28 (1): 43–58.

Morton, R., 1992. Fish assemblages in residential canal developments near the mouth of a subtropical Queensland estuary Marine and Freshwater Research 43, 1359–1371.

Peterson, R.N., W.C. Burnett, M. Taniguchi, J. Chen, I.R. Santos, and S. Misra. 2008. Determination of transport rates in the Yellow River–Bohai Sea mixing zone via natural geochemical tracers. *Continental Shelf Research* 28 (19): 2700–2707.

Reef, R., I.C. Feller, and C.E. Lovelock. 2010. Nutrition of mangroves. *Tree Physiology* 30 (9): 1148–1160.

Ridd, P.V. 1996. Flow through animal burrows in mangrove creeks. *Journal of Estuarine, Coastal and Shelf Science* 43 (5): 617–625.

Rivera-Monroy, V.H., R.R. Twilley, R.G. Boustany, J.W. Day, F. Vera-Herrera, and M. del Carmen Ramirez. 1995. Direct denitrification in mangrove sediments in Terminos Lagoon, Mexico. *Marine Ecology Progress Series* 126: 97–109.

Robinson, C., B. Gibbes, and L. Li. 2006. Driving mechanisms for groundwater flow and salt transport in a subterranean estuary. *Geophysical Research Letters* 33: 3402.

Robinson, C.E., P. Xin, I.R. Santos, M.A. Charette, L. Li, and D.A. Barry. 2018. Groundwater dynamics in subterranean estuaries of coastal unconfined aquifers: controls on submarine groundwater discharge and chemical inputs to the ocean. *Advances in Water Resources* 115: 315–331.

Rufí-Salís, M., J. Garcia-Orellana, G. Cantero, J. Castillo, A. Hierro, J. Rieradevall, and J. Bach. 2019. Influence of land use changes on submarine groundwater discharge. *Environmental Research Communications* 1 (3): 031005.

Sadat-Noori, M., I.R. Santos, C.J. Sanders, L.M. Sanders, and D.T. Maher. 2015. Groundwater discharge into an estuary using spatially distributed radon time series and radium isotopes. *Journal of Hydrology* 528: 703–719.

Sadat-Noori, M., I.R. Santos, D.R. Tait, M.J. Reading, and C.J. Sanders. 2017. High porewater exchange in a mangrove-dominated estuary revealed from short-lived radium isotopes. *Journal of Hydrology* 553: 188–198.

Sanders, C.J., I.R. Santos, R. Barcellos, and E.V. Silva Filho. 2012. Elevated concentrations of dissolved Ba, Fe and Mn in a mangrove subterranean estuary: consequence of sea level rise? *Continental Shelf Research* 43: 86–94.

Sanders, C.J., B.D. Eyre, I.R. Santos, W. Machado, W. Luiz-Silva, J.M. Smoak, J.L. Breithaupt, M.E. Ketterer, L. Sanders, H. Marotta, and E. Silva-Filho. 2014. Elevated rates of organic carbon, nitrogen, and phosphorus accumulation in a highly impacted mangrove wetland. *Geophysical Research Letters* 41 (7): 2475–2480.

Sanders, C.J., Maher, D.T., Tait, D.R., Williams, D., Holloway, C., Sippo, J.Z., Santos, I.R., 2016. Are global mangrove carbon stocks driven by rainfall? Journal of Geophysical Research. Biogeosciences 121, 2600–2609.

Santos, I.R., N. Dimova, R.N. Peterson, B. Mwashote, J. Chanton, and W.C. Burnett. 2009. Extended time series measurements of submarine groundwater discharge tracers (222Rn and CH4) at a coastal site in Florida. *Marine Chemistry* 113 (1-2): 137–147.

Santos, I.R., R.N. Peterson, B.D. Eyre, and W.C. Burnett. 2010. Significant lateral inputs of fresh groundwater into a stratified tropical estuary: evidence from radon and radium isotopes. *Marine Chemistry* 121 (1-4): 37–48.

Santos, I.R., J. de Weys, D.R. Tait, and B.D. Eyre. 2013. The contribution of groundwater discharge to nutrient exports from a coastal catchment: post-flood seepage increases estuarine N/P ratios. *Estuaries and Coasts* 36 (1): 56–73.

Santos, I.R., K.R. Bryan, C.A. Pilditch, and D.R. Tait. 2014. Influence of porewater exchange on nutrient dynamics in two New Zealand estuarine intertidal flats. *Marine Chemistry* 167: 57–70.

Santos, I.R., D.T. Maher, R. Larkin, J.R. Webb, and C.J. Sanders. 2019. Carbon outwelling and outgassing vs. burial in an estuarine tidal creek surrounded by mangrove and saltmarsh wetlands. *Limnology and Oceanography* 9999: 1–18.

Schmidt, A., Gibson, J., Santos, I.R., Schubert, M., Tattrie, K., Weiss, H., 2010. The contribution of groundwater discharge to the overall water budget of two typical Boreal lakes in Alberta/Canada estimated from a radon mass balance. *Journal of Hydrology Earth System Sciences* 14, 79–89.

Schwendenman, L., R. Riecke, and R.J. Lara. 2006. Solute dynamics in a North Brazilian mangrove: the influence of sediment permeability and freshwater input. *Wetlands Ecology and Management* 14 (5): 463–475.

Singh, G., A. Ramanathan, and M.B.K. Prasad. 2005. Nutrient cycling in mangrove ecosystem: a brief overview. *International Journal of Ecology and Environmental Sciences* 30: 231–244.

Smith, V.H. 2006. Responses of estuarine and coastal marine phytoplankton to nitrogen and phosphorus enrichment. *Limnology and Oceanography* 51 (1part2): 377–384.

Smith, C.G., and P.W. Swarzenski. 2012. An investigation of submarine groundwater—borne nutrient fluxes to the west Florida shelf and recurrent harmful algal blooms. *Limnology and Oceanography* 57 (2): 471–485.

Smith, C.G., R.M. Price, P.W. Swarzenski, and J.C. Stalker. 2016. The role of ocean tides on groundwater-surface water exchange in a mangrove-dominated estuary: Shark River Slough, Florida Coastal Everglades, USA. *Estuaries and Coasts* 39 (6): 1600–1616.

Stewart, B.T., I.R. Santos, R.D. Tait, P.A. Macklin, and D.T. Maher. 2015. Submarine groundwater discharge and associated fluxes of alkalinity and dissolved carbon into Moreton Bay (Australia) estimated via radium isotopes. *Marine Chemistry* 174: 1–12.

Stieglitz, T.C., J.F. Clark, and G.J. Hancock. 2013. The mangrove pump: the tidal flushing of animal burrows in a tropical mangrove forest determined from radionuclide budgets. *Geochimica et Cosmochimica Acta* 102: 12–22.

Stocker, L., N. Harvey, and S.J. Metcalf. 2016. Management of coastal canal estates in Australia: challenges and opportunities. *Ocean & Coastal Management* 130: 148–161.

Su, N., J. Du, W.S. Moore, S. Liu, and J. Zhang. 2011. An examination of groundwater discharge and the associated nutrient fluxes into the estuaries of eastern Hainan Island, China using 226Ra. *Science of the Total Environment* 409 (19): 3909–3918.

Susilo, A., P.V. Ridd, and S. Thomas. 2005. Comparison between tidally driven groundwater flow and flushing of animal burrows in tropical mangrove swamps. *Wetlands Ecology and Management* 13 (4): 377–388.

Taillardat, P., P. Willemsen, C. Marchand, D.A. Friess, D. Widory, P. Baudron, V.V. Truong, T.-N. Nguyễn, and A.D. Ziegler. 2018. Assessing the contribution of porewater discharge in carbon export and CO2 evasion in a mangrove tidal creek (Can Gio, Vietnam). *Journal of Hydrology* 563: 303–318.

Taillardat, P., A.D. Ziegler, D.A. Friess, D. Widory, F. David, N. Ohte, T. Nakamura, J. Evaristo, N. Thanh-Nho, T. Van Vinh, and C. Marchand. 2019. Assessing nutrient dynamics in mangrove porewater and adjacent tidal creek using nitrate dual-stable isotopes: a new approach to challenge the Outwelling Hypothesis? *Marine Chemistry* 214: 103662.

Tait, D.R., D.T. Maher, P.A. Macklin, and I.R. Santos. 2016. Mangrove pore water exchange across a latitudinal gradient. *Geophysical Research Letters* 43 (7): 3334–3341.

Tait, D.R., D.T. Maher, C.J. Sanders, and I.R. Santos. 2017. Radium-derived porewater exchange and dissolved N and P fluxes in mangroves. *Geochimica et Cosmochimica Acta* 200: 295–309.

Taniguchi, M., H. Dulai, K.M. Burnett, I.R. Santos, R. Sugimoto, T. Stieglitz, G. Kim, N. Moosdorf, and W.C. Burnett, W.C. 2019. Submarine Groundwater Discharge: Updates on Its Measurement Techniques, Geophysical Drivers, Magnitudes, and Effects. *Frontiers in Environmental Science* 7(141): https://doi.org/10.3389/fenvs.2019.00141.

Taylor, G.D., T.D. Fletcher, T.H. Wong, P.F. Breen, and H.P. Duncan. 2005. Nitrogen composition in urban runoff—implications for stormwater management. *Water Research* 39 (10): 1982–1989.

Trent, W.L., Pullen, E.J., Moore, D., 1972. Waterfront housing developments: their effect on the ecology of a Texas estuarine area.

Wadnerkar, P.D., I.R. Santos, A. Looman, C.J. Sanders, S. White, J.P. Tucker, and C. Holloway. 2019. Significant nitrate attenuation in a mangrove-fringed estuary during a flood-chase experiment. *Environmental Pollution* 253: 1000–1008.

Wang, X., and J. Du. 2016. Submarine groundwater discharge into typical tropical lagoons: a case study in eastern Hainan Island, China.*Geochemical, Geophysics, Geosystems* 17: 4366–4382.

Wang, M., J. Zhang, Z. Tu, X. Gao, and W. Wang. 2010. Maintenance of estuarine water quality by mangroves occurs during flood periods: a case study of a subtropical mangrove wetland. *Marine Pollution Bulletin* 60 (11): 2154–2160.

Wang, F., N. Chen, J. Yan, J. Lin, W. Guo, P. Cheng, Q. Liu, B. Huang, and Y. Tian. 2019. Major processes shaping mangroves as inorganic nitrogen sources or sinks: insights from a multidisciplinary study. *Journal of Geophysical Research: Biogeosciences* 124 (5): 1194–1208.

Webb, J.R., I.R. Santos, B. Robson, B. Macdonald, L. Jeffrey, and D.T. Maher. 2017. Constraining the annual groundwater contribution to the water balance of an agricultural floodplain using radon: The importance of floods. *Water Resources Research* 53 (1): 544–562.

Webb, J.R., I.R. Santos, D.T. Maher, D.R. Tait, T. Cyronak, M. Sadat-Noori, P. Macklin, and L.C. Jeffrey. 2019. Groundwater as a source of dissolved organic matter to coastal waters: insights from radon and CDOM observations in 12 shallow coastal systems. *Limnology and Oceanography* 64 (1): 182–196.

White, S.A., I.R. Santos, and S. Hessey. 2018. Nitrate loads in subtropical headwater streams driven by intensive horticulture. *Environmental Pollution* 243 (Pt B): 1036–1046.

Xia, Y.Q., and H.L. Li. 2012. A combined field and modeling study of groundwater flow in a tidal marsh. *Hydrology and Earth System Sciences* 16 (3): 741–759.

Xiao, K., J. Wu, H. Li, Y. Hong, A.M. Wilson, J.J. Jiao, and M. Shananan. 2018. Nitrogen fate in a subtropical mangrove swamp: potential association with seawater-groundwater exchange. *Science of the Total Environment* 635: 586–597.

Xiao, K., H. Li, M. Shananan, X. Zhang, X. Wang, Y. Zhang, X. Zhang, and H. Liu. 2019a. Coastal water quality assessment and groundwater transport in a subtropical mangrove swamp in Daya Bay, China. *Science of the Total Environment* 646: 1419–1432.

Xiao, K., A.M. Wilson, H. Li, and C. Ryan. 2019b. Crab burrows as preferential flow conduits for groundwater flow and transport in salt marshes: a modeling study. *Advances in Water Resources* 132: 103408.

Xin, P., G. Jin, L. Li, and D.A. Barry. 2009. Effects of crab burrows on pore water flows in salt marshes. *Advances in Water Resources* 32 (3): 439–449.

Zedler, J.B., and S. Kercher. 2005. Wetland resources: status, trends, ecosystem services, and restorability. *Annual Review of Environment and Resources* 30 (1): 39–74.

Zhang, Y., L. Li, D.V. Erler, I. Santos, and D. Lockington. 2017. Effects of beach slope breaks on nearshore groundwater dynamics. *Hydrological Processes* 31 (14): 2530–2540.